Synthesis, Structure, Electrochemistry, and Magnetism of [$Mn^{III}Mn^{III}$], [$Mn^{III}Fe^{III}$] and [$Fe^{III}Fe^{III}$] Cores: Generation of Phenoxyl Radical Containing [$Fe^{III}Fe^{III}$] Species

Cláudio Nazari Verani,[a] Eberhard Bothe,[a] Dirk Burdinski,[a] Thomas Weyhermüller,[a] Ulrich Flörke,[b] and Phalguni Chaudhuri*[a]

Dedicated to Prof. H.-J. Haupt on the occasion of his 65th birthday

Keywords: N,O ligands / Electrochemistry / Manganese / Iron / Radicals / Magnetic properties

Neutral homo- and heterobinuclear complexes with the general formula [(tmtacn)M_A(salox)$_3M_B$] where M_A (Mn^{III} or Fe^{III}) is facially coordinated to the cyclic amine 1,4,7-trimethyl-1,4,7-triazacyclononane (tmtacn) and M_B (Mn^{III} or Fe^{III}) is coordinated to the azomethine nitrogens and phenolate oxygens of the bridging ligand, salicylaldoxime, thus yielding $M_AN_3O_3$ and $M_BN_3O_3$ cores. The compounds were characterized by IR, UV/Vis, mass spectrometry, Mössbauer spectroscopy, electrochemistry, and variable-temperature (2–295 K) magnetic susceptibility measurements. The molecular structures of the compounds [(tmtacn)Fe^{III}(salox)$_3$-Fe^{III}] (**3**) and [(tmtacn)Fe^{III}(*t*BuSalox)$_3Fe^{III}$] (**4**) were established by X-ray diffraction. Three oximate groups –HC=N–O bridge the metal centers with Fe···Fe separations of 3.571(1) and 3.486(1) Å for (**3**) and (**4**), respectively. Analysis of the susceptibility data yields antiferromagnetic interactions between the metal centers for the complexes $Fe^{III}Fe^{III}$ and Mn^{III}-Fe^{III}, but a ferromagnetic interaction for $Mn^{III}Mn^{III}$. The electrochemistry of all complexes was investigated in detail. For the complexes $Fe^{III}Fe^{III}$ (**3**) and (**4**) a series of reversible one-electron transfer waves leads to the formation of the cations $[Fe_2]^{1+/2+/3+}$ that are attributed to the generation of salox-based phenoxyl radicals.

Introduction

Current interest in the coordination chemistry of phenol containing ligands[1−4] is mainly due to the discovery of the widespread occurrence of tyrosinase radicals in metalloproteins, involved in oxygen-dependent enzymatic radical catalysis.[5−8] Amongst the catalytically essential redox-active amino acids, glycyl, cysteinyl, tryptophan, tyrosyl, and modified tyrosyl are the most prevalent, and tyrosine-based radical enzymes are the best characterized.

As part of an effort directed toward the development of biologically inspired homogeneous catalysis[9−11] for the aerial oxidation of organic substrates like alcohols and amines, we are investigating the synthesis and reactivity of phenolate complexes of the transition metals, together with their one-electron oxidized phenoxyl radical complexes. Such phenoxyl radical complexes, stable in the solid state, are rather rare. This scarcity is partly due to the fact that the metal−phenolate bond to a late transition metal ion should be relatively weak. For the early transition metal ions, the metal−phenolate bonding is strengthened by π-donation from the lone pair of electrons on oxygen into an empty d-orbital on the metal, but for the late transition metal ions such empty low-lying orbitals are not always available.

In another field of modern coordination chemistry there is a continuous interest in polynuclear exchange-coupled systems that are relevant to the area of both magnetic materials[12−15] and biomodeling.[5,16−18] Of special interest in this context is the rational synthesis of polynuclear complexes with desired nuclearity by reaction of mono or dinuclear complexes with different metal complexes[19] of the same or different nature, i.e. the use of metal complexes as ligands.

In this regard we have reported several series of linear complexes comprising [M_A-M_B], [$M_A-M_B-M_A$], [$M_A-M_B-M_C$], and [$M_A-M_B-M_B-M_A$] cores,[20−23] involving the end-capping amine tmtacn and several bridging oximes together with nonlinear tetranuclear [$(M_A)_2(\mu$-$O)_2(M_B)_2$] complexes containing salicylaldoxime, *salox*.[24]

Although salicylaldoxime was used as a complexing agent as early as 1930,[25] comparatively few reports on its ligating properties towards the trivalent transition metal ions have been published.[24,26−30] During the course of the preparative work involving M^{III}(saloxH)$_3$, where M = Fe^{III}, Mn^{III}, saloxH = the monoanion of salicylaldoxime H_2salox, we envisaged the possibility of preparing a series of neutral dinuclear complexes with the general formula [(tmtacn)M_A(salox)$_3M_B$], where M_A = Mn^{III} or Fe^{III}, and is facially coordinated to the cyclic amine 1,4,7-trimethyl-1,4,7-triazacyclononane, *tmtacn*, and M_B = Mn^{III} or Fe^{III} and is coordinated to the three salox units.

[a] Max-Planck-Institut für Strahlenchemie,
Stiftstrasse 34−36, 45470 Mülheim an der Ruhr, Germany
E-mail: chaudh@mpi-muelheim.mpg.de
[b] Anorganische und Analytische Chemie, Universität Gesamthochschule,
D-33098 Paderborn, Germany

  1434−1948/01/0808−2161 $ 17.50+.50/0

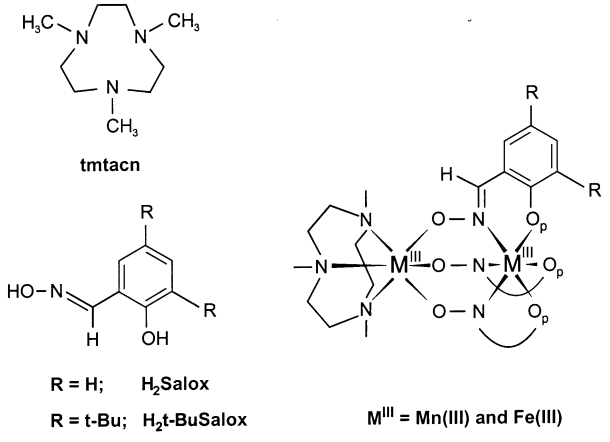

Scheme 1. Ligands and general frame of the [(*tmtacn*) M_A (*salox*)$_3$ M_B] complexes

It has been recently established by Wieghardt et al.[31] that *tert*-butyl substituents at the *ortho* and *para* positions of the phenolates facilitate one-electron oxidation to the corresponding phenoxyl radicals, because these substituents decrease the oxidation potential of the phenolates and provide enough steric bulk to suppress bimolecular decay reactions. Accordingly, we have synthesized salicylaldoxime with *tert*-butyl substituents at the *ortho* and *para* positions i.e., 4,6-di-*tert*-butyl salicylaldoxime, abbreviated *tBu-salox*, and investigated the electrochemical behavior amongst other studies, to generate the phenoxyl radical species from the parent dinuclear Fe^{III} complex. Thus, the compounds [(tmtacn)Mn^{III}(salox)$_3$$Mn^{III}$] (**1**), [(tmtacn)$Mn^{III}$(salox)$_3$$Fe^{III}$] (**2**), [(tmtacn)$Fe^{III}$(salox)$_3$$Fe^{III}$] (**3**), and [(tmtacn)$Fe^{III}$(*t*Bu-salox)$_3$$Fe^{III}$] (**4**), were synthesized and characterized by means of various spectroscopic methods. The single crystal X-ray structure determinations of (**3**) and (**4**) were also performed.

Results and Discussion

The complexes [(tmtacn)M_A(salox)$_3$$M_B$] were obtained by reaction of an appropriate metal salt with the ligand H_2salox in oxygen-free methanol, in the presence of triethylamine, followed either by the solid [Fe(tmtacn)Cl_3] or [(tmtacn)$_2$$Mn^{III}_2$(μ-O)(μ-OAc)$_2$]$^{2+}$, produced in situ, in stoichiometric equivalents. Dark microcrystalline products were collected with yields varying between 40 to 70%. Satisfactory analyses (C, H, N, Fe, Mn) were obtained. Our attempts to characterize the species produced by the reaction of salicylaldoxime with either $FeCl_3$ or "Mn^{III} acetate" are yet to be successful. However, these species are able to yield the dinuclear complexes **1**, **2**, **3**, and **4**, in the presence of a base (Et_3N) and the [M(tmtacn)]$^{3+}$ unit [M = Fe^{III} or Mn^{III}]. The function of the added base is to provide a medium needed for deprotonation of the −HC=N−OH groups present.

Since the IR spectra of complexes **1**, **2**, **3**, and **4** are quite similar, the discussion is confined to the most important vibrations of the 4000−400 cm^{-1} region in relation to the structure. The free ligands, H_2salox and 4,6-*t*Bu-H_2salox, have intense sharp absorptions at 3411 and 3438 cm^{-1}, attributed to the ν(OH) vibrations of the phenolic and enolic groups, respectively. This absorption is missing in the spectra of the dinuclear complexes, indicating that the phenolic and enolic protons are lost on chelation. The very intense band at 1619 cm^{-1} for H_2salox and a medium intense at 1609 cm^{-1} for 4,6-*t*Bu-H_2salox are assigned to the $\nu_{(C=N)}$ vibration mode. These bands shift to ca. 1592 cm^{-1} for **1**−**4**. The medium strong band at ca. 1150−1170 cm^{-1} for the free oxime ligands shifts slightly (ca. 5 cm^{-1}) to higher frequency for all dinuclear complexes and has been assigned to the $\nu_{(N=O)}$ vibration of the oxime groups. Finally, a set of intense and medium-intensity peaks between 3007 and 2864 cm^{-1} is present in both ligand 4,6-*t*Bu-H_2salox and complex **4** and reveals the presence of the *tert*-butyl groups.

Mass spectrometry in the ESI positive mode has been proved to be a very useful analytical tool for characterization of complexes **1**−**4**. Homometal complexes **1**, **3**, and **4** provide the respective molecular ion peaks with the expected isotope ratios in the ESI positive mode as the base peaks (100%), but the heterometal complex, **2** fails to provide the molecule peak as the base peak; the latter is observed at *m*/*z* = 710, and can be assigned to the ion [M + Na]$^+$.

The optical spectra of **1**, **2**, and **3** in MeCN have been measured in the 350−1200 nm wavelength range. Only one maximum is observed for each complex: for **1** at 571 nm (ε = 2820 L mol^{-1} cm^{-1}), for **2** at 501 nm (ε = 5880 L mol^{-1} cm^{-1}), and for **3** at 486 nm (ε = 7844 L mol^{-1} cm^{-1}). As these transitions are unusually intense for a high-spin Mn^{III} or Fe^{III} d-d transition, they are assigned to a phenolate-to-M^{III} [M^{III} = Fe or Mn] transition. Thus these bands can be assigned to a transition from pπ orbitals on the phenolate oxygen atoms to the dπ* orbitals on M^{III}.[32−35] The expected ligand field transitions, $^6A_1 \rightarrow {}^4T_2$ (^4G) for Fe^{III} and $^5E_g \rightarrow {}^5T_{2g}$ for Mn^{III}, which are likely to

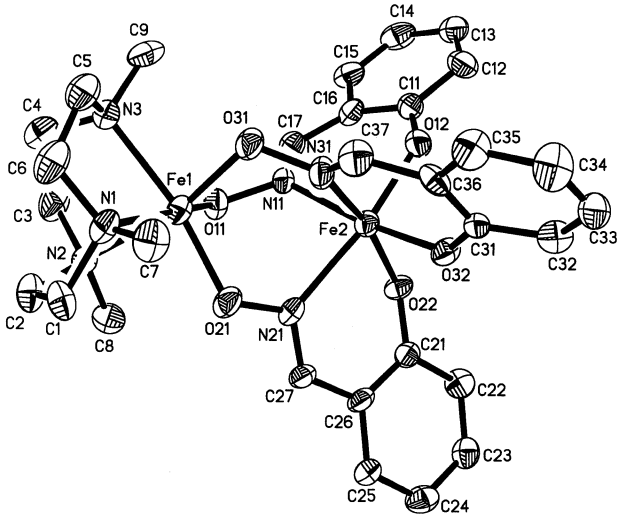

Figure 1. Molecular structure of the dinuclear $Fe^{III}Fe^{III}$ core in **3**, showing the atom-numbering scheme

occur in the 500−700 nm region, are obscured by the more intense charge transfer phenolate-to-metal (III) transition.

Molecular Structure of [(tmtacn)Fe^{III}(salox)$_3Fe^{III}$]·MeOH (3) and of [(tmtacn)Fe^{III}(*t*Bu-salox)$_3Fe^{III}$]·3.5 $CHCl_3$ (4)

The structures of the neutral complexes in crystals of **3** and **4** were determined, and as expected they are identical with respect to the coordination geometry of the Fe^{III} centers. Hence we are refraining from describing both structures in detail, and accordingly the ORTEP for **3** is shown in Figure 1. Table 1 lists selected bond lengths and angles for both **3** and **4**.

The coordination geometry of Fe(1) is distorted octahedral with three nitrogen atoms, N(1), N(2), and N(3), from the facially coordinated tridentate macrocyclic amine, and three oxygen atoms O(11), O(21), and O(31) from the bridging oximate groups. The Fe(1)−N (average 2.22 Å) and Fe(1)−O (average 1.94 Å) correspond to those of the known values[36,37] for Fe^{III} complexes with this macrocyclic amine, and are in agreement with a d^5 high-spin electron configuration of the Fe^{III}-center. A deviation from the idealized orthogonal geometry is found for the ligand tmtacn, the N−Fe(1)−N angles ranging between 78.6° and 79.3°, whereas O−Fe(1)−O angles fall between 96.1° and 99.6°. The Fe(1) is displaced by 0.10 Å from the mean basal plane comprising N(1)N(3)O(11)O(21) atoms, toward the apical oxygen atom O(31) of the oximate group. The ligand tmtacn exhibits no unexpected features.

The Fe(2) center is also six-fold coordinated. Coordination occurs facially through three phenolate oxygen atoms, O(12), O(22), and O(32), and three azomethine nitrogen atoms, N(11), N(21), and N(31), from the salox ligands. The average Fe(2)−N and Fe(2)−O bond lengths, 2.16 Å and 1.94 Å, respectively, fall within the ranges that are consid-

Table 1. Selected bond lengths [Å] and angles [°] for **3** and **4**

[(tmtacn)Fe^{III}(salox)$_3Fe^{III}$] (**3**)		[(tmtacn)Fe^{III}(4,6-*t*Bu-salox)$_3Fe^{III}$] (**4**)	
Fe(1)−N(1)	2.225(9)	Fe(1)−N(1)	2.249(2)
Fe(1)−N(2)	2.224(8)		
Fe(1)−N(3)	2.222(8)		
Fe(1)−O(11)	1.948(6)		
Fe(1)−O(21)	1.935(7)	Fe(1)−O(2)	1.930(2)
Fe(1)−O(31)	1.934(6)		
Fe(2)−N(11)	2.144(7)		
Fe(2)−N(21)	2.199(8)	Fe(2)−N(2)	2.141(2)
Fe(2)−N(31)	2.136(8)		
Fe(2)−O(12)	1.951(6)	Fe(2)−O(1)	1.931(2)
Fe(2)−O(22)	1.942(6)		
Fe(2)−O(32)	1.911(6)		
N(1)−Fe(1)−N(2)	79.3(3)		
N(2)−Fe(1)−N(3)	78.6(3)		
N(2)−Fe(1)−O(11)	85.1(3)	O(2)−Fe(1)−O(2)#2	100.16(7)
N(1)−Fe(1)−O(21)	88.1(3)	O(2)#1−Fe(1)−N(1)	93.89(8)
N(3)−Fe(1)−O(21)	166.7(3)	O(2)−Fe(1)−N(1)	85.70(8)
N(1)−Fe(1)−O(31)	95.0(3)		
N(3)−Fe(1)−O(31)	87.5(3)		
O(21)−Fe(1)−O(31)	96.9(3)	O(2)−Fe(1)−N(1)#1	163.50(8)
O(12)−Fe(2)−O(22)	95.8(3)		
O(12)−Fe(2)N(21)	168.7(3)		
O(22)−Fe(2)−N(21)	83.7(3)		
N(11)−Fe(2)−O(32)	171.9(3)	O(2)−Fe(1)−N(1)#2	93.89(8)
N(21)−Fe(2)−O(32)	98.1(3)		
N(11)−Fe(2)−N(31)	88.4(3)	N(1)−Fe(1)−N(1)#2	78.49(9)
N(21)−Fe(2)−N(31)	83.4(3)		
N(1)−Fe(1)−N(3)	79.0(3)	O(1)−Fe(2)−O(1)#2	95.78(7)
N(1)−Fe(1)−O(11)	164.3(3)		
N(3)−Fe(1)−O(11)	95.5(3)	O(1)Fe(2)−N(2)#1	83.46(7)
N(2)−Fe(1)O(21)	96.0(3)		
O(11)−Fe(1)−O(21)	96.1(3)	O(1)#2−Fe(2)−N(2)#1	171.29(8)
N(2)−Fe(1)−O(31)	165.8(3)	O(1)−Fe(2)−N(2)	92.93(8)
O(11)−Fe(1)−O(31)	99.6(3)	O(1)#1−Fe(2)−N(2)	171.30(8)
O(12)−Fe(2)−N(11)	83.6(3)		
N(11)Fe(2)−O(22)	97.3(3)	N(2)#1−Fe(2)−N(2)	87.92(8)
N(11)−Fe(2)−N(21)	85.2(3)		
O(12)−Fe(2)−O(32)	93.2(3)		
O(22)−Fe(2)−O(32)	90.4(3)		
O(12)−Fe(2)−N(31)	98.1(3)		
O(22)−Fe(2)−N(31)	165.5(3)		
O(32)−Fe(2)−N(31)	84.6(3)		

ered as normal covalent bonds for Fe^{III} centers with a d^5 high-spin electronic configuration.[29,30] The largest deviation from idealized 90° inter-bond angles is 6.3°, which occurs within the six-membered N−Fe(2)−O−C−C−C chelate rings, the N−Fe(2)−N angles ranging between 88.4° and 83.4°, whereas the O−Fe(2)−O angles fall between 90.4° and 95.8°. The Fe(2) lies practically on the best basal plane comprising N(11)N(21)O(12)O(32) atoms, and is displaced only 0.08 Å above the plane toward the apical atom O(22) of a phenolate group. Thus, the metrical parameters of the Fe(2) center in **3** are very similar in magnitude to the Fe(1) center and to those reported earlier for the FeN_3O_3 core.[37]

The binuclear skeleton is not coplanar, but is bent with a Fe(1)···Fe(2) separation of 3.570(1) Å. The dihedral angle between the planes Fe(1)N(1)N(3)O(11)O(21) and Fe(2)N(11)N(21)O(12)O(32) is 109.8°.

The deviation from octahedral symmetry for the Fe(1) and Fe(2) centers has been evaluated from the twist angle (60° for an ideal octahedral and 0° for a trigonal prismatic arrangement). The $Fe(2)N_3O_3$ core is more trigonally distorted than the $Fe(1)N_3O_3$ core. The N_3O_3 donor atoms are arranged around the Fe(2) center with a twist angle of 49.2°, whereas for the Fe(1) center the twist angle is 51.1°. In other words, the coordination polyhedron around Fe(2) is 10.8° away from the octahedral symmetry.

The N−O (average 1.38 Å) and C=N (average 1.28 Å) bond lengths and C−N−O bond angle (average 113.4°) of the bridging salicylaldoxime ligand are found to be very similar to those of other comparable structures.[38−39]

The structure determinations for **3** and **4** unambiguously show that, in both structures, the oxidation level of all iron centers is +3 with d^5 high-spin electron configuration.

Table 1 compares the important bond lengths in both salox complexes. It can be easily observed that in **3** these distances are slightly longer than those in complex **4**. This general trend can be explained by considering that the *tert*-butyl groups act in both inductive (+I) and mesomeric (+M) fashion as electron-donors. It implies that the substituted salox complex **4** provides a more electron-rich coordination environment and consequently the interaction between donor atoms (O, N) and iron is stronger, producing a small but significant shortening of the bond lengths.

Mössbauer Spectroscopy and Magnetic Susceptibility Measurements

The 3+ oxidation state and the high spin electronic configuration of the iron centers in complexes **2** and **3** were confirmed by Mössbauer spectroscopy.[40] The spectra were measured at 80 K and zero-field. They consist of asymmetrical quadrupole doublets with isomer-shifts (δ) of 0.530 mms^{-1} for **2**, 0.566 mms^{-1} and 0.451 mms^{-1} for **3**, and quadrupole splitting (ΔE_Q) of 0.350 for **2**, 0.261 and 0.175 mms^{-1} for **3**.

The Mössbauer spectra have provided us with another piece of important information. Examination of the literature values[41] for the isomer-shifts (ΔE_Q) of the Fe^{III}-center that is capped by the tmtacn ligand shows that the ΔE_Q values lie within the range 0.44 to 0.47 mms^{-1}. Thus the isomer shifts of 0.530 for **2** and 0.566 mms^{-1} for **3** are attributed to the Fe^{III} centers coordinated to the phenolate oxygen and azomethine nitrogen atoms of the salicylaldoxime ligand. This establishes that the Mn^{III} center in **2** is coordinated to the macrocyclic tmtacn ligand. In other words, the fact that the metal ions have remained associated with their different ligands originating from their respective starting materials and practically no scrambling of the ligands has occurred, are evidenced by the Mössbauer experiments.

Magnetic susceptibility data for polycrystalline samples of **1**, **2**, **3**, and **4** were collected in the temperature range 2 to 290 K and the magnetic parameters are listed in Table 2. The spin Hamiltonian $\mathbf{H} = -2\boldsymbol{J}\cdot\boldsymbol{S_1}\cdot\boldsymbol{S_2}$ with $S_1 = S_2 = 2$ for **1**, $S_1 = 2$, $S_2 = {}^5/_2$ for **2**, and $S_1 = S_2 = {}^5/_2$ for **3** and **4** is used throughout.

Table 2. Magnetochemical data for complexes **1** to **4**

Compound	J [cm^{-1}]	$g_1 = g_2$	θ [K]	PI
[(tmtacn)$\mathbf{Mn^{III}}$(salox)$_3$$\mathbf{Mn^{III}}$] (**1**)	+6.5	2.07	−0.43	–
[(tmtacn)$\mathbf{Mn^{III}}$(salox)$_3$$\mathbf{Fe^{III}}$] (**2**)	−4.8	2.03	–	0.06
[(tmtacn)$\mathbf{Fe^{III}}$ (salox)$_3$$\mathbf{Fe^{III}}$] (**3**)	−11.8	2.00	–	–
[(tmtacn)$\mathbf{Fe^{III}}$(*t*Bu-salox)$_3$$\mathbf{Fe^{III}}$] (**4**)	−12.2	2.07	–	–

The effective magnetic moment for **1** increases monotonically with decreasing temperature until a plateau is reached at 20−15 K with an μ_{eff} value of 9.11 μ_B (Figure 2). Below 15 K μ_{eff} starts to decrease reaching a value of 8.4 μ_B at 2 K. The temperature behavior of μ_{eff} for **1**, Mn^{III} Mn^{III}, is characteristic of a ferromagnetic exchange coupling between two high-spin d^4 Mn^{III} ions. The data could be fitted using the Heisenberg−Dirac−van Vleck (HDvV) model and the least-squares fitting computer program Julius-F[42] with a full-matrix diagonalization approach. The best fit was obtained with $J = +6.5$ cm^{-1}, $g = 2.07$ and $\theta = -0.43$ K and is shown in Figure 2.

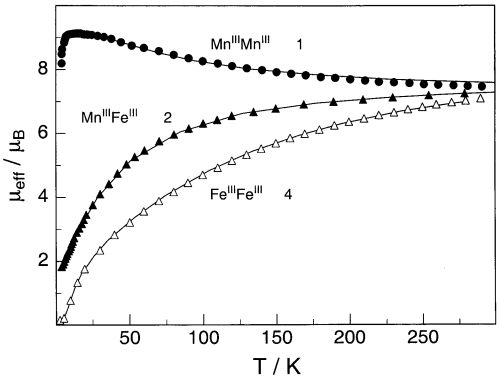

Figure 2. Plots of μ_{eff} vs. temperature for **1**, **2**, and **4**. Temperature-dependence of μ_{eff} of **3** is nearly identical to that of **4**. The solid lines represent the best fits to the spin Hamiltonian $H = -2J\cdot S_1\cdot S_2$ (see text)

For complex **2** the temperature dependence of the effective magnetic moment shows a monotonic decrease from 7.25 μ_B at 275 K to 1.85 μ_B at 4 K. This is typical of an

Table 3. Electrochemical data for complexes **1** to **4**; all potentials in Volts referred to Fc^+/Fc in CH_3CN ($E_{1/2}$ = 0.081 V)

Compound	$E_{1/2}$ (ox3)	$E_{1/2}$ (ox2)	$E_{1/2}$ (ox1)	$E_{1/2}$ (red1)	$E_{1/2}$ (red2)
[(tmtacn)**Mn^{III}**$(salox)_3$ **Mn^{III}**] (**1**)	–	0.30	−0.28	−0.86	−1.30
[(tmtacn)**Mn^{III}**$(salox)_3$ **Fe^{III}**] (**2**)	–	–	−0.19	−0.89	−1.81
[(tmtacn)**Fe^{III}** $(salox)_3$ **Fe^{III}**] (**3**)	0.97	0.77	0.41	−1.32	−1.86
[(tmtacn)**Fe^{III}**(tBu-salox)$_3$ **Fe^{III}**] (**4**)	0.89	0.47	0.31	−1.37	−2.08

antiferromagnetically coupled two-spin system with total spin ground state $S_t = {}^1/_2$ arising from $S_{Mn} = 2$ and $S_{Fe} = {}^5/_2$. Temperature independent paramagnetism (TIP) of $400 \cdot 10^{-6}$ cm^3 mol^{-1} and a monomeric impurity (6%, $S = 2$) were considered to account for the excess magnetic moment of the sample at 4 K. Fitting for the isotropic exchange yielded $J = -4.8$ cm^{-1} and $g = 2.03$ (Figure 2).

The magnetic behaviors of complexes **3** and **4** are, as expected, nearly identical, and hence they will be treated together. On lowering the temperature, the effective magnetic moments decrease monotonically for both complexes. Representative μ_{eff} values for complexes **3** and **4** (given in brackets) are 6.86 μ_B (7.09 μ_B) at 290 K, 4.68 μ_B (4.70 μ_B) at 100 K, 0.24 μ_B (0.21 μ_B) at 5 K, and 0.16 μ_B (0.15 μ_B) at 2 K, indicating a diamagnetic ground state $S_t = 0$ for both **3** and **4**. This arises from antiparallel spin coupling between two Fe^{III} centers with $S = {}^5/_2$. Simulation of the data yielded $J = -11.8$ cm^{-1}, $g_1 = g_2 = 2.00$ for **3** and $J = -12.2$ cm^{-1}, $g_1 = g_2 = 2.07$ for **4**. It was not necessary to consider terms for TIP or paramagnetic impurity in the simulation procedure. The experimental data together with the simulation for complex **4** are shown in Figure 2.

Electro- and Spectroelectrochemistry

Complexes **1**−**4** were submitted to electrochemical studies in order to characterize the nature of its redox processes. Table 3 summarizes the results, and Figure 3 and Figure 4 show representative examples of the electrochemical measurements.

The cyclic voltammogram of [(tmtacn)$Mn^{III}$$(salox)_3Mn^{III}$] (**1**) shows four consecutive reversible one-electron-transfer waves (Figure 3), which are detected with scan rates varying from 20 to 500 mVs^{-1} at +0.30 V, −0.28 V, −0.86 V, and −1.30 V versus Fc^+/Fc. The oxidation processes at +0.30 V and −0.28 V are assigned to the following equilibria shown in Equation (1).

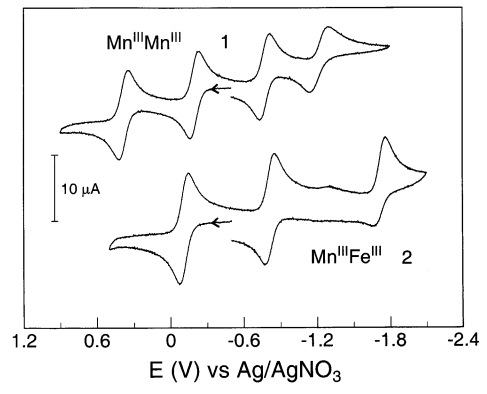

Figure 3. Cyclic voltammograms of **1** (top) and **2** (bottom) in CH_3CN (0.10 M $[(nBu_4)N]PF_6$ at a glassy carbon electrode; scan rate: 200 mV/s; complex ≈ 10^{-3} M; 298 K)

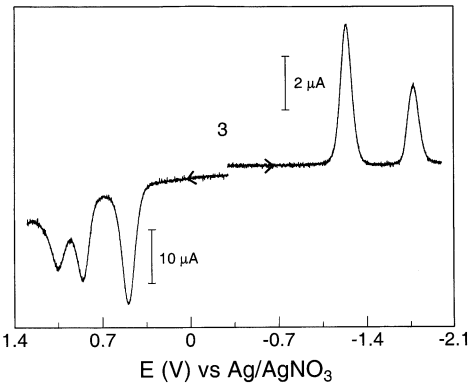

Figure 4. Square wave voltammograms for oxidation and reduction of **3** in MeCN, 0.1 M $[TBA]PF_6$. Oxidation: 0.25 mm Pt working electrode (WE), scan frequency 3000 Hz. Reduction: 2 mm GC WE, 5 Hz

$$\begin{array}{l} [(tmtacn)Mn^{III}(salox)_3Mn^{III}]^0 \\ \quad\quad \mathbf{1} \\ E_{1/2}(ox1) \quad -1e^- \downarrow\uparrow +1e^- \\ [(tmtacn)Mn^{IV}(salox)_3Mn^{III}]^+ \\ E_{1/2}(ox2) \quad -1e^- \downarrow\uparrow +1e^- \\ [(tmtacn)Mn^{IV}(salox)_3Mn^{IV}]^{2+} \end{array} \quad (1)$$

Electrochemically-reversible one-electron-transfer steps preclude any significant structural rearrangement during these oxidation processes, i.e., no change in the actual framework of the structures for all three species has occurred. The electrochemical behavior of complex **1** in the more negative potential range (−0.4 to −2.0 V vs. Ag/$AgNO_3$) can be assigned to the following redox scheme shown in Equation (2), on the basis of earlier reports.[21]

$$\begin{array}{l} [(tmtacn)Mn^{II}(salox)_3Mn^{II}]^{2-} \\ E_{1/2}(red2) \quad -1e^- \downarrow\uparrow +1e^- \\ [(tmtacn)Mn^{II}(salox)_3Mn^{III}]^- \\ E_{1/2}(red1) \quad -1e^- \downarrow\uparrow +1e^- \\ [(tmtacn)Mn^{III}(salox)_3Mn^{III}]^0 \\ \quad\quad \mathbf{1} \end{array} \quad (2)$$

The CV of **2** (Figure 3) exhibits two reversible one-electron waves at −0.19 V and −0.89 V versus Fc^+/Fc, and one quasi-reversible cathodic wave at more negative potentials that may be attributed to the reduction of iron center coordinated with phenolate and azomethine nitrogen atoms of the salicylaldoxime. Controlled-potential coulometry established a one-electron transfer process for the reversible cases. The following equilibria are thus involved during the manganese-centered electron-transfer processes (Equation 3).

$$
\begin{array}{l}
[(tmtacn)Mn^{III}(salox)_3Fe^{III}]^0 \\
\mathbf{2} \\
E_{1/2}(ox1) \quad -1e^- \downarrow\uparrow +1e^- \\
[(tmtacn)Mn^{IV}(salox)_3Fe^{III}]^+ \\
[(tmtacn)Mn^{III}(salox)_3Fe^{III}]^0 \\
\mathbf{2} \\
E_{1/2}(red1) \quad -1e^- \uparrow\downarrow +1e^- \\
[(tmtacn)Mn^{II}(salox)_3Fe^{III}]^- \\
E_{1/2}(red2) \quad -1e^- \uparrow\downarrow +1e^- \\
[(tmtacn)Mn^{II}(salox)_3Fe^{II}]^{2-}
\end{array}
\qquad (3)
$$

Complex **3** in MeCN exhibits five redox processes. The voltammetric waves of two of them, at +0.41 V and at −1.32 V versus Fc^+/Fc show reversible appearance under "standard" conditions (2 mm working electrode and scan rates of 0.05−0.5 V/s in CV and about 60 Hz in square wave voltammetry, SQW). Controlled potential coulometry at the appropriate potentials reveals that these waves originate from a one-electron oxidation and a one-electron reduction, respectively. The oxidation must be ligand-centered, and the reduction is assigned to an Fe^{III}/Fe^{II} couple. Two further (ligand-centered) oxidations at +0.77 and +0.97V and one more reduction at −1.86 V (assigned to reduction of the second iron) are detectable by SQW. The second reduction is best seen at relatively slow scan frequencies (< 10 Hz) most probably due to its slow heterogeneous electron transfer step. The two additional oxidations are detectable only at much higher frequencies (> 1000 Hz) because of rapid homogeneous following-up reactions. The results for the oxidations and reductions are displayed in Figure 4.

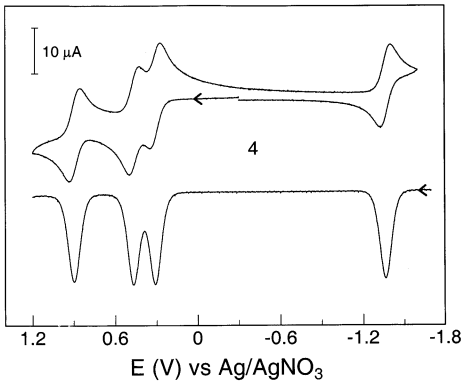

Figure 5. Square wave voltammogram (at 20 Hz) and CV (at 0.2 V/s) of **4** in MeCN, 0.1 M [TBA]PF_6

For complex **4** in MeCN, four reversible one electron waves were observed at the following potentials: +0.89, +0.47, +0.31, and −1.37 V, versus Fc^+/Fc. Additionally, an irreversible wave at $E_p^{ox} = -2.08$ V versus Fc^+/Fc is also found (Figure 5). The two reductive waves at −1.37 V and −2.08 V versus Fc^+/Fc are attributed to processes centered on the metal centers as described in Equation (4a), whereas the three oxidation waves are attributed to successive ligand-centered phenoxyl-radical formation [Equation (4b)]. The overall redox processes are given below where ($salox^\bullet$) represents a salox-based phenoxyl-radical.

reductive processes

$$
\begin{array}{l}
[(tmtacn)Fe^{II}(t\text{Bu-salox})_3Fe^{II}]^{2-} \\
E_{1/2}(red2) \quad -1e^- \downarrow\uparrow +1e^- \\
[(tmtacn)Fe^{II}(t\text{Bu-salox})_3Fe^{III}]^{1-} \\
E_{1/2}(red1) \quad -1e^- \downarrow\uparrow +1e^- \\
[(tmtacn)Fe^{III}(t\text{Bu-salox})_3Fe^{III}]^0 \\
\mathbf{4}
\end{array}
\qquad (4a)
$$

oxidative processes

$$
\begin{array}{l}
[(tmtacn)Fe^{III}(t\text{Bu-salox})_3Fe^{III}]^0 \\
\mathbf{4} \\
E_{1/2}(ox1) \quad -1e^- \downarrow\uparrow +1e^- \\
[(tmtacn)Fe^{III}(t\text{Bu-salox})_2(t\text{Bu-salox}^\bullet)Fe^{III}]^+ \\
E_{1/2}(ox2) \quad -1e^- \downarrow\uparrow +1e^- \\
[(tmtacn)Fe^{III}(t\text{Bu-salox})(t\text{Bu-salox}^\bullet)_2Fe^{III}]^{2+} \\
E_{1/2}(ox3) \quad -1e^- \downarrow\uparrow +1e^- \\
[(tmtacn)Fe^{III}(t\text{Bu-salox}^\bullet)_3Fe^{III}]^{3+}
\end{array}
\qquad (4b)
$$

Each of these waves involves a $1e^-$-transfer, as detected by coulometry at fixed potentials. Both complexes **3** and **4** contain two high spin Fe^{III} ions in an octahedral *fac*-N_3O_3 donor set, but complex **4** in MeCN exhibits two additional ligand-centered reversible oxidation processes absent in **3**, as shown in Figure 5.

Spectroelectrochemical experiments were performed intending to isolate and characterize (by EPR spectroscopy) the resulting oxidized complexes. As the electron transfer processes during coulometric measurements at appropriately fixed potentials at ambient temperature has been found to be too slow (>> $^1/_2$ h), characterization of the radical complexes by UV/Vis and EPR spectroscopy has not been possible. Lowering the temperature of the experiments was also not effective, and the measurements resulted

Table 4. Crystallographic data for **3**·MeOH and **4**·3.5 $CHCl_3$

	[(tmtacn)Fe^{III}(salox)$_3Fe^{III}$] **3**·MeOH	[(tmtacn)Fe^{III}(4,6-*t*Bu-salox)$_3Fe^{III}$] **4**·3.5 $CHCl_3$
Empirical formula	$C_{30}H_{36}Fe_2N_6O_6 \cdot CH_3OH$	$C_{54}H_{84}Fe_2N_6O_6 \cdot 3.5\ CHCl_3$
Molecular weight	720.39	1442.76
Temperature	293(2) K	100(2) K
Wavelength	0.71073 Å	0.71073 Å
Crystal system	orthorhombic	trigonal
Space group	$P2_12_12_1$	$P\bar{3}$
Unit cell dimensions	a = 12.105(5) Å	a = 17.341(2) Å α = 90°
	b = 15.655(5) Å	b = 17.341(2) Å β = 90°
	c = 17.374(7) Å	c = 13.656(2) Å γ = 120°
Volume	3292(2) Å^3	3556.3(8) Å^3
Z	4	2
Density (calculated)	1.453 Mg/m^3	1.347 Mg/m^3
Absorption coefficient	0.936 mm^{-1}	0.851 mm^{-1}
F(000)	1504	1506
Crystal size	0.40 × 0.09 × 0.08 mm^3	0.67 × 0.49 × 0.42 mm^3
Color	dark red needle	deep violet
Diffractometer used	Siemens R3m/V	Siemens SMART
θ range for data collection	2.34 to 27.56°	2.02 to 30.00°
Index ranges	$0 \le h \le 15$	$-24 \le h \le 26$
	$0 \le k \le 20$	$-21 \le k \le 26$
	$0 \le l \le 22$	$-19 \le l \le 20$
Reflections collected	4237	35066
Independent reflections	4237	6851 [R_{int} = 0.0358]
Refinement method	Full-matrix least-squares on F^2	Full-matrix least-squares on F^2
Data/restraints/parameters	4237/0/418	6617/0/266
Goodness-of-fit on F^2	0.854	1.170
Absolute structure parameter	0.02(4)	-
Final R indices [$I > 2\sigma(I)$]	$R1$ = 0.0551, $wR2$ = 0.0976	$R1$ = 0.0605, $wR2$ = 0.1378
R indices (all data)	$R1$ = 0.1363, $wR2$ = 0.1353	$R1$ = 0.0750, $wR2$ = 0.1475

in ill-defined isosbestic points. Nevertheless, the growth of peaks around 420−450 nm (ε ≈ 10580 $M^{-1}cm^{-1}$) serves as a strong indication for the radical nature of the generated complexes.

Concluding Remarks

The results summarized here for **3** and **4** suggest the generation of three ligand-centered oxidation processes, attributable to phenoxyl-radicals, rather than the formation of unusually high oxidation states at the central iron centres. On the contrary, in case of manganese, facile oxidation of metal centres rather than the ligands occurs. In contrast to the general notion that azomethine N-donor sets stabilize the 2+ oxidation state of iron centers, salicylaldoxime as a ligand with coordinated phenolato and azomethine groups enormously stabilizes 3+ oxidation state in such metal centers. This is a general feature of the phenolato iron complexes.

Experimental Section

Solvents and reagents were obtained from commercial sources and used without further purification. The synthon [Fe(tmtacn)]Cl_3[37] and the cyclic amine 1,4,7-trimethyl-1,4,7-triazacyclononane, tmtacn[43] were prepared according to previous published methods. − Infrared spectra were measured from 4000 to 400 cm^{-1} as KBr pellets at room temperature on a Perkin−Elmer FT-IR-Spectrophotometer 2000. − C, H, N, and metal content of the compounds were determined by the Microanalytical Laboratory of the Ruhr-Universität Bochum. − UV/Visible spectra of $5.0 \cdot 10^{-4}$ M solution in MeCN were recorded on a Perkin−Elmer UV/Vis Spectrophotometer Lambda 19 in the range 200−1200 nm. − Cyclic voltammetry and square wave voltammetry experiments were performed using an EG&G Potentiostat/Galvanostat 273A. A standard three-electrode-cell was employed with a glassy-carbon working electrode, a platinum-wire auxiliary electrode, and a $Ag/AgNO_3$ reference electrode. Measurements were made under an inert atmosphere at room temperature. All the potentials are referenced to Fc^+/Fc as the internal standard. − The magnetochemical measurements of the powdered samples were performed in a Quantum Design SQUID-Magnetometer MPMS in a field of 1 T. The samples were put in gelatine-capsules, and the response function was measured four times for each 32 measured temperature points. Diamagnetic contributions were estimated for each compound by making use of Pascal's constants. − Mössbauer data were recorded on alternating constant-acceleration spectrometers. The minimal experimental linewidth was 0.24 mms^{-1} full width at half maximum. The sample temperature was kept constant at 80 K either in an Oxford Variox or an Oxford Mössbauer-Spectromag cryostat. $^{57}Co/Rh$ was used as the radiation source. The measurements were carried out with solid samples containing the isotope ^{57}Fe and the isomer shifts are given relative to α-Fe at room temperature.

X-ray Crystallography: The crystallographic data of [LFe(salox)$_3$Fe] (**3**) and [LFe(*t*Bu-salox)$_3$Fe] (**4**) are summarized in Table 4.

Graphite monochromated Mo-K_α radiation (λ = 0.71073 Å) was used throughout. Intensity data were corrected for Lorentz-Polarization and absorption effects using the program SADABS.[44] The structures were solved by direct methods using SHELXTL plus.[45] The function minimized during full-matrix least-squares refinement was $\Sigma w(|F_o| - |F_c|)^2$. Hydrogen atoms attached to carbon were placed at calculated positions and refined as riding atoms with isotropic thermal parameters. All non-hydrogen atoms were refined with anisotropic thermal parameters. Crystallographic data (excluding structure factors) for the structure reported in this paper have been deposited with the Cambridge Crystallographic Data Centre as supplementary publication number CCDC-151864. Copies of the data can be obtained free of charge on application to the CCDC, 12 Union Road, Cambridge CB2 1EZ, U.K. [Fax: (internat.) + 44-1223/336-033; E-mail: deposit@ccdc.cam.uk].

Preparation of the Compounds

Salicylaldoxime (H_2salox): was prepared by heating a solution of salicylaldehyde and free hydroxylamine in EtOH for 0.5 h under reflux. The yellowish white solid obtained on cooling was recrystallized from EtOH. Purity of the sample was checked by comparing its spectroscopic properties with those of the material salicylaldoxime available on the market.

4,6-Di-*tert*-butylsalicylaldoxime (4,6-*t*Bu-H_2salox): In a round bottom flask hydroxylamine−hydrochloride (5.6 g: 80 mmol) was dissolved in 10 mL of distilled water. Simultaneously, 4,6-di-*tert*-butylsalicylaldehyde (5.0 g: 20 mmol) was dissolved in 40 mL of warm MeOH. Both solutions were mixed and heated gently for 1 h under reflux. On cooling, a white product was isolated and washed with distilled water. M.p. 130−134 °C; yield 5.10 g (96%).− $C_{15}H_{23}NO_2$ (249.4): calcd. C 72.25, H 9.30, N 5.62; found C 72.5, H 9.4, N 5.4. − ^{1}H NMR [250 MHz, $CDCl_3$, 300 K] δ/ppm = 1.28; 1.42 [2 × s, 2 × 9 H (*t*Bu)], 6.98 [s, 1 H (H−ON)], 7.09; 7.35 [2 × s, 2 × 1 H (H-Ar)], 8.22 [s, 1 H (H−O−Ar)], 10.02 [s, 1H (H−C-Ar)]. − EI-MS: m/z = 249 $[M]^+$ and 234 $[M - CH_3]^+$ (100%).

[(*tmtacn*)Mn^{III}(*salox*)$_3Mn^{III}$] (1): A solution of the cyclic amine (0.17 g; 1 mmol) in 40 mL of MeOH was treated with a sample of manganese(III) acetate (0.52 g; 2 mmol) under vigorous stirring in an atmosphere of argon. After 0.5 h the resulting red-brown solution was charged with a sample of salicylaldoxime (0.41 g; 3 mmol) and 1 mL of triethylamine. The very dark solution was heated under reflux for 1 h, followed by a filtration to get rid of some green solid, presumably, Mn(Hsalox)$_3$. The solution kept at room temperature provided deep brown (almost black) crystals. The crystals were collected by filtration and air-dried. Yield 350 mg (≈50%). − $C_{30}H_{36}Mn_2N_6O_6$ (686.5): calcd. C 52.26, H 5.26, N 12.19, Mn 15.94; found C 52.0, H 5.3, N 12.3, Mn 16.0. − MS (ESI-positive in CH_3CN): m/z = 686 $[M]^+$ (100%).

[(tmtacn)Mn^{III}(salox)$_3Fe^{III}$] (2): A solution of the cyclic amine (0.17 g; 1 mmol) in 40 mL of MeOH was treated with a sample of manganese(III) acetate (0.52 g; 2 mmol) under vigorous stirring in an atmosphere of argon. After 0.5 h the resulting red-brown solution was charged with a suspension of $FeCl_3$ (0.16 g; 1 mmol) and salicylaldoxime (0.41 g; 3 mmol) in MeOH (30 mL) containing 1 mL of triethylamine. The very dark solution was heated under reflux for 2 h and then filtered to remove any solid particles. The solution kept at room temperature provided a deep brown solid. Deep brown crystals were obtained by diffusion of n-pentane into a MeCN solution of the solid. The crystals were collected by filtration and air-dried. Yield 270 mg (≈40%). − $C_{30}H_{36}FeMnN_6O_6$ (687.4): calcd. C 52.19, H 5.28, N 12.20, Mn 7.99, Fe 8.12; found C 52.3, H 5.2, N 12.1, Mn 7.8, Fe 8.1. − MS (ESI-positive in CH_3CN): m/z = 688 $[M + H]^+$ (75%), 710 $[M + Na]^+$ (100%).

[(tmtacn)Fe^{III}(salox)$_3Fe^{III}$]·MeOH (3): $FeCl_3$ (0.16 g; 1 mmol) was added to a degassed solution of salicylaldoxime (0.41 g; 3 mmol) in dry MeOH (50 mL) containing 1 mL of triethylamine under vigorous stirring. The resulting suspension was stirred at room temperature for 1 h and then charged with a solid sample of [Fe(tmtacn)Cl_3][37] (0.33 g; 1.0 mmol) and gently heated under reflux for 1 h. The resulting dark brown solid was collected by filtration and air-dried. X-ray quality crystals as dark red needles were obtained by diffusion of MeOH into a MeCN solution of **3**. Yield 450 mg (≈62%). − $C_{31}H_{40}N_6O_7Fe_2$ (720.4): calcd. C 51.69, H 5.60, N 11.67, Fe = 15.53; found C 52.0, H 5.5, N 11.6, Fe 15.3. − MS (ESI-positive in CH_3CN): m/z = 689 (100%) $[M + H]^+$.

[(tmtacn)Fe^{III}(*t*Busalox)$_3Fe^{III}$]·3.5 $CHCl_3$ (4): [Fe(tmtacn)Cl_3] (0.33 g; 1.0 mL) was added to a degassed solution of 4,6-di-*tert*-butylsalicylaldoxime (0.75 g; 3 mmol) in MeOH (50 mL) containing 0.84 mL of triethylamine under vigorous stirring. A solid sample of $FeCl_3$ (0.16 g; 1 mmol) was added and the resulting dark-red solution was stirred for further 0.5 h under gentle reflux. The solution kept at room temperature provided a dark-red microcrystalline solid, which was collected by filtration and air-dried. Yield 710 mg (≈70%). − $C_{54}H_{84}Fe_2N_6O_6$ (1025.0): calcd. C 63.28, H 8.26, N 8.20, Fe 10.9; C 62.9, H 8.2, N 8.2, Fe 10.8. − MS (ESI-positive in CH_3CN): a single peak at m/z = 1025 (100%) $[M + H]^+$. Recrystallization from $CHCl_3$ yielded X-ray quality crystals.

Acknowledgments

The authors thank the Fonds der Chemischen Industrie and the Max-Planck-Society for financial support. C. N. V. thanks DAAD for a fellowship. Technical assistance of Mrs. H. Schucht and Mrs. P. Höfer is gratefully acknowledged. Our thanks are also due to R. Werner and W. Haase (Darmstadt) and J. Bonvoisin (Toulouse) for the preliminary susceptibility measurements.

[1] For example: J. A. Halfen, B. A. Jzdzewski, S. Mahapatra, L. M. Berreau, E. C. Wilkinson, L. Que Jr., W. B. Tolman, *J. Am. Chem. Soc.* **1997**, *119*, 8217−8227.
[2] Y. Wang, T. D. P. Stack, *J. Am. Chem. Soc.* **1996**, *118*, 13097−13098.
[3] D. Zurita, I. Gautier-Luneau, S. Menage, J. L. Pierre, E. Saint-Aman, *J. Biol. Inorg. Chem.* **1997**, *2*, 46−55.
[4] E. Bill, J. Müller, T. Weyhermüller, K. Wieghardt, *Inorg. Chem.* **1999**, *38*, 5795−5802 and references therein.
[5] R. H. Holm, E. I. Solomon, Guest Editors, *Chem. Rev.* **1996**, no. 7, *96*.
[6] *Metal Ions in Biological Systems* (Ed.: H. Sigel, A. Sigel), **1994**, Vol. 30.
[7] G. T. Babcock, M. Espe, C. Hoganson, N. Lydakis-Simantiris, J. McCracken, W. Shi, S. Styring, C. Tommas, K. Warncke, *Acta Chem. Scand.* **1997**, *51*, 533−540.
[8] J. Stubbe, W. A. van der Donk, *Chem. Rev.* **1998**, *98*, 705−762.
[9] P. Chaudhuri, M. Hess, U. Flörke, K. Wieghardt, *Angew. Chem. Int. Ed.* **1998**, *110*, 2217−2220.
[10] P. Chaudhuri, M. Hess, T. Weyhermüller, K. Wieghardt, *Angew. Chem. Int. Ed.* **1999**, *38*, 1095−1098.
[11] P. Chaudhuri, M. Hess, J. Müller, K. Hildenbrand, E. Bill, T. Weyhermüller, K. Wieghardt, *J. Am. Chem. Soc.* **1999**, *119*, 9599−9610.
[12] O. Kahn, *Molecular Magnetism*, VCH Verlagsgesellschaft: Weinheim, Germany, **1993**.
[13] *Research Frontiers in Magnetochemistry* (Ed.: C. J. O'Connor), World Scientific, Singapore, **1993**.

[14] *Magnetic Molecular Materials* (Eds.: D. Gatteschi, O. Kahn, J. S. Miller, F. Palacio), Kluwer Academic Publishers: Dordrecht, The Netherlands, **1991**.
[15] *Magneto-Structural Correlations in Exchange Coupled Systems* (Eds.: R. D. Willett, D. Gatteschi, O. Kahn), Kluwer Academic Publishers: Dordrecht, The Netherlands, **1985**.
[16] S. J. Lippard, J. M. Berg, *Principles of Bioinorganic Chemistry*, University Science Books, CF **1994**.
[17] *Bioinorganic Chemistry of Copper* (Eds.: K. D. Karlin, Z. Tyeklár), Chapman & Hall, New York **1993**.
[18] W. Kaim, B. Schwederski, *Bioanorganische Chemie*, B. G. Teubner, Stuttgart **1991**.
[19] O. Kahn, *Adv. Inorg. Chem.* **1995**, *43*, 179−259.
[20] D. Burdinski, F. Birkelbach, T. Weyhermüller, U. Flörke, H.-J. Haupt, M. Lengen, A. X. Trautwein, E. Bill, K. Wieghardt, P. Chaudhuri, *Inorg. Chem.* **1998**, *37*, 1009−1020.
[21] F. Birkelbach, U. Flörke, H.-J. Haupt, C. Butzlaff, A. X. Trautwein, K. Wieghardt, P. Chaudhuri, *Inorg. Chem.* **1998**, *37*, 2000−2008 and references therein.
[22] C. N. Verani, E. Rentschler, T. Weyhermüller, E. Bill, P. Chaudhuri, *J. Chem. Soc., Dalton Trans.* **2000**, 251−258 and references therein.
[23] C. Krebs, M. Winter, T. Weyhermüller, E. Bill, K. Wieghardt, P. Chaudhuri, *J. Chem. Soc., Chem. Commun.* **1995**, 1913−1915 and references therein.
[24] P. Chaudhuri, F. Birkelbach, M. Winter, V. Staemmler, P. Fleischhauer, W. Haase, U. Flörke, H.-J. Haupt, *J. Chem. Soc., Dalton Trans.* **1994**, 2313−2319 and references therein.
[25] F. Epharain, *Ber. Dtsch. Chem. Ges.* **1930**, *63*, 1928−1930.
[26] S. J. Rettig, A. Storr, J. Trotler, *Acta Crystallogr., Sect. C* **1992**, *48*, 1587−1590.
[27] E. Toyota, K. Umakoshi, Y. Yamamoto, *Bull. Chem. Soc. Jpn.* **1995**, *68*, 858−865.
[28] K. R. Manolov, *Russ. J. Inorg. Chem.* **1967**, *12*, 1431−1434.
[29] J. M. Thorpe, R. L. Beddoes, D. Collison, C. D. Garner, M. Helliwell, J. M. Holmes, P. A. Tasker, *Angew. Chem. Int. Ed.* **1999**, *38*, 1119−1121.
[30] E. Bill, C. Krebs, M. Winter, M. Gerdan, A. X. Trautwein, U. Flörke, H.-J. Haupt, P. Chaudhuri, *Chem. Eur. J.* **1997**, *3*, 193−201.
[31] B. Adam, E. Bill, E. Bothe, B. Goerdt, G. Haselhorst, K. Hildenbrand, A. Sokolowski, S. Steenken, T. Weyhermüller, K. Wieghardt, *Chem. Eur. J.* **1997**, *3*, 308−319.
[32] B. P. Gaber, V. Miskowski, T. G. Spiro, *J. Am. Chem. Soc.* **1974**, *96*, 6868−6873.
[33] P. Chaudhuri, M. Winter, F. Birkelbach, P. Fleischhauer, W. Haase, U. Flörke, H.-J. Haupt, *Inorg. Chem.* **1991**, *30*, 4291−4293.
[34] U. Auerbach, U. Eckert, K. Wieghardt, B. Nuber, J. Weiss, *Inorg. Chem.* **1990**, *29*, 938−944.
[35] S. K. Chandra, P. Basu, D. Ray, S. Pal, A. Chakravorty, *Inorg. Chem.* **1990**, *29*, 2423−2428.
[36] P. Chaudhuri, *Proc. Indian Acad. Sci (Chem. Sci)* **1999**, *111*, 397−411.
[37] P. Chaudhuri, M. Winter, K. Wieghardt, S. Gehring, W. Haase, B. Nuber, J. Weiss, *Inorg. Chem.* **1988**, *27*, 1564−1569.
[38] P. L. Orioli, E. C. Lingafelter, B. W. Brown, *Acta Crystallogr.* **1964**, *17*, 1113−1118.
[39] H. Saarainen, J. Korvenranta, E. Näsäkkälä, *Acta Chem. Scand., Ser. A* **1980**, *34*, 443−448 and references therein.
[40] N. N. Greenwood, T. C. Gibb, *Mössbauer Spectroscopy*, Chapman and Hall, London, **1971**.
[41] H. Hummel, Dissertation, Bochum, **1998** and references therein.
[42] F. Birkelbach, C. Krebs, V. Staemmler, Bochum, unpublished.
[43] K. Wieghardt, P. Chaudhuri, B. Nuber, J. Weiss, *Inorg. Chem.* **1982**, *21*, 3086−3090.
[44] G. M. Sheldrick, *SADABS*, University of Göttingen, **1994**.
[45] G. M. Sheldrick, *SHELXTL PLUS*, Siemens Analytical X-ray Instruments, Madison, WI, **1990**.

Received November 2, 2000
[I00417]